Mon. Not. R. astr. Soc. (1987) **226,** 461–471

IRAS observations of NGC 1333

R. E. Jennings, D. H. M. Cameron, W. Cudlip and C. J. Hirst *Department of Physics and Astronomy, University College London, Gower Street, London WC1E 6BT*

Accepted 1986 December 23. Received 1986 December 18; in original form 1986 October 6

Summary. *IRAS* CPC observations of a region measuring 25×25 arcmin^2 in the NGC 1333 molecular cloud have revealed nine distinct far-infrared sources, many of which have not previously been reported, with luminosities ranging from 3 to 161 $L_\odot$. Some are known to be associated with very young, pre-main-sequence stars and are important in understanding the production mechanisms of the Herbig–Haro objects found in their vicinity.

1 Introduction

The region lying south of the reflection nebula NGC 1333 is known to be associated with active star formation and contains many near- and far-IR sources embedded in a molecular cloud in which CO observations have shown that there are high-velocity bipolar outflows of gas. The stages in stellar evolution represented range from heavily embedded pre-main-sequence stars through to main-sequence late-type B stars almost completely free of their parental cloud. The region has a considerable number of Herbig–Haro (HH) objects and while it is of interest to determine their driving sources, this is not always possible due to the complexity of the region.

This paper reports far-IR observations of an area of about 625 arcmin^2 using the Chopped Photometric Channel (CPC) aboard the infrared satellite *IRAS*. The main aims of the observations were:

(i) To locate and measure the luminosity of the stars powering the HH objects in the region.
(ii) To search for proto-stars, i.e. stars in the collapse phase of their evolution.

Previous observations of this region in the far-IR have been made from the NASA *Kuiper Airborne Observatory* by Harvey, Wilking & Joy (1984) who published a map at 100 μm showing the four principal sources. They also give the energy distribution of each of these sources in the range from 1 to 160 μm. The *IRAS* CPC data reveal a further five far-IR sources.

Many references to observations at other wavelengths, which are relevant to the study of this region, are given in the paper by Harvey *et al.* (1984). There are also a number of recent papers which include maps of the HH 7–11 complex in the $S(1)$ emission line of molecular hydrogen at

2.12 μm (Zealey, Williams & Sandell 1984) and also in the Q-branch lines around 2.42 μm (Lightfoot & Glencross 1986).

2 Observations

The *IRAS* Chopped Photometric Channel (CPC) had two channels at wavelengths of 50 and 100 μm. A single aperture of 1.2 arcmin was chopped against a cold reference blade in order to modulate the incoming radiation and provide an absolute reference. Although the sensitivity of the CPC was not as high as that of the *IRAS* survey detectors [10σ sensitivities were 7.0 Jy at both 50 and 100 μm for the CPC, compared with 0.85 and 3.0 Jy for the Survey Array 60 and 100 μm channels respectively (Neugebauer *et al.* 1984)], it had the advantage of higher spatial resolution. A more detailed description of the CPC can be found in the paper by Wildeman, Beintema & Wesselius (1983).

A single CPC observation consisted of an 18 leg raster scan covering an area of about 9×9 arcmin^2. The in-scan data were averaged to give a sample spacing of 0.5 arcmin and, in the final post-mission processing, the data were cleaned (i.e. detector spikes removed), gain corrected and interpolated on to a uniform 0.5 arcmin grid aligned with the local directions of RA and dec. Nine such observations were required to cover the 25 arcmin square box observed and each observation was repeated.

3 Data reduction

The nine frames and their repeats were checked for inconsistencies before being combined to form a single map, 25×25 arcmin^2, for each of the two wavebands. Differences, of a few per cent, between the background signals in adjacent 100 μm frames were observed, resulting mainly from time- and flux-dependent sensitivity variations of the CPC detectors (Wesselius *et al.* 1985). These discrepancies were minimized with the use of a background normalization procedure which consisted of offsetting the data such that the lowest 10 per cent of the pixels in each frame had the same mean value. This problem did not arise in the case of the 50-μm maps.

A temperature map was derived by calculating a temperature, T, for each pixel from the ratio of the flux densities F_1 and F_2 (Jy) at corresponding wavelengths λ_1 and λ_2 (50 and 100 μm), assuming a dust emissivity proportional to ν, when

$$T \approx \frac{hc\left(\frac{\lambda_2-\lambda_1}{\lambda_2\lambda_1}\right)}{k\ln\left[\frac{F_2}{F_1}\left(\frac{\lambda_2}{\lambda_1}\right)^4\right]}.$$

The nine sources identified in this region can be seen on the 50 and 100 μm maps (Figs 1 and 2), but due to the presence of IR cirrus the sources appear less distinct on the 100 μm map. The major discrepancy between the detections in the two bands is an area of emission to the east of the main sources on the 100 μm map. This may well be due to the presence of very cold dust in this region.

Before measuring the flux from the individual sources, a maximum entropy deconvolution procedure was applied to the data to help remove the point spread function. This process did not affect the total flux but helped to delineate the sources. The flux at each wavelength was obtained by summing the relevant pixels and subtracting the local background. The total IR flux was then calculated using the temperatures already deduced.

The usual distance assigned to NGC 1333 of 500 pc is based on photometry of BD+30°549, a B9V type star (Strom, Grasdalen & Strom 1974), which illuminates this portion of the dark

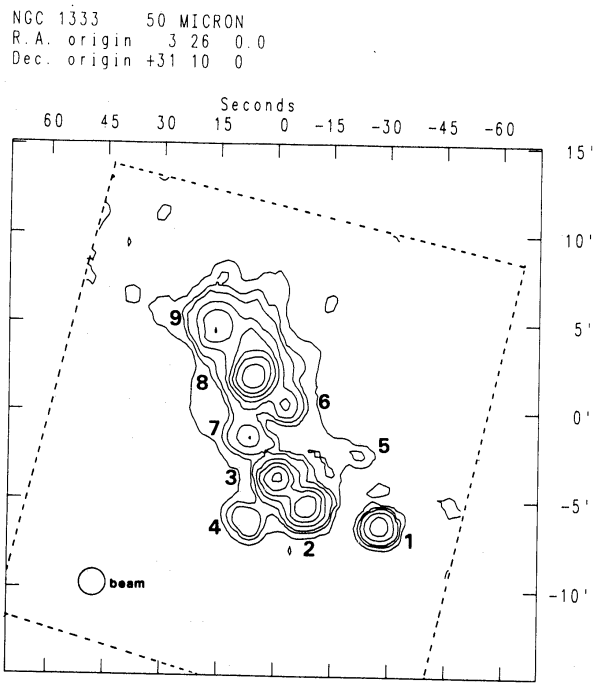

Figure 1. CPC channel 1 (50 μm) flux map. The area scanned by the CPC is indicated by the dotted box. Contour levels are 80, 100, 180, 270, 400, 600, 910 and 1370 MJy Ster^{-1}.

cloud B205. However, more recent evidence presented by Herbig & Jones (1983) suggests that a distance of 350 pc is more appropriate and this has been adopted here. It is assumed that all the sources are at approximately the same distance since this part of the sky does not lie in the galactic plane and chance coincidences are unlikely.

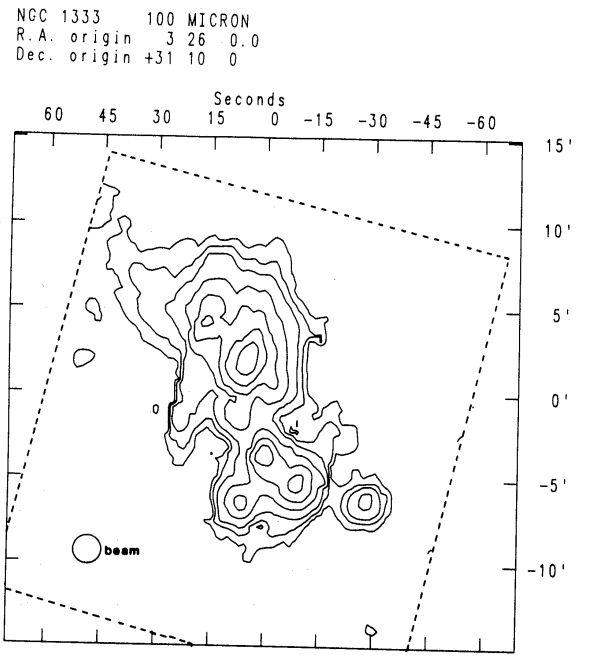

Figure 2. CPC channel 2 (100 μm) flux map. Contour levels are 170, 200, 250, 380, 575, 860, 1290 and 1950 MJy Ster^{-1}.

4 Results

The CPC data are presented in Table 1, the sources being listed as *IRAS* 1 etc. and any relevant associations being given. Table 2 is an extract from the *IRAS Point Source Catalog* (Beichman *et al.* 1985) for the region scanned by the CPC detectors. This catalogue was compiled using data from the survey detectors onboard *IRAS* which provided information in four wavebands at 12, 25, 60 and 100 μm. The catalogue revealed eight sources in the region discussed here, six of which are in the vicinity of CPC flux peaks. The accuracy of the point source fluxes is limited by confusion with nearby neighbouring sources and, at longer wavelengths, by the presence of IR cirrus. This problem of confusion is illustrated by the fact that four of the point sources in this region have been assigned, prior to colour correction, identical 100 μm fluxes of 946.7 Jy. The extent of such confusion in a particular region of the sky can be deduced from the data quality flags which accompany each flux measurement. Comparison of the 60 and 100 μm survey and the 50 and 100 μm CPC bands reveals reasonable agreement when the confusion and quality flags make such a comparison valid.

As previously mentioned, maps at 50 and 100 μm of the region are shown in Figs 1 and 2. Fig. 3 is the temperature map derived as described above. Fig. 4 is a flux–flux plot of the nine CPC sources in the region; this is an alternative way of presenting the data and its significance is discussed below. Plate 1 is an optical photograph of the region showing the location of the Herbig–Haro objects; using the position of stars seen on the photograph, sufficient 50 μm contours have been superimposed to identify the CPC sources discussed and the point source detections in this area, as listed in the *IRAS* catalogue, are indicated.

5 Discussion

The NGC 1333 region contains many previously identified IR sources, Herbig–Haro objects and water masers. Here we are primarily concerned with establishing the relationship between IR pre-main-sequence stars and nearby associations of Herbig–Haro objects which are generally accepted to be tracers of the outflow from such stars. [A general treatment of molecular outflows is given in the review by Lada (1985)]. While some of the Herbig–Haro objects are single and isolated, the majority are contained in the three regions HH 7–11, 12 and 6.

5.1 HH 7–11

The environment surrounding Herbig–Haro objects 7–11 (see Plate 1) has been studied extensively in the optical, IR and radio. With the exception of HH 9, optical observations show that the objects HH 7–11 lie essentially in a straight line (Mundt 1985). Lightfoot & Glencross (1986) have recently proposed a model explaining the observed pattern of Herbig–Haro objects, including HH 9, as being the result of a highly collimated precessing jet interacting with the ambient molecular material. The energizing source for HH 7–11 is the young stars SSV 13 which is positioned at the HH 11 end of the chain of HH objects and corresponds to the source *IRAS* 3. The presence of this star was originally deduced from IR observations (e.g. Strom, Vrba & Strom 1976), and more recently it has been detected in red CCD images obtained by Liseau (1985). He gives its coordinates as $\alpha = 03^{h}25^{m}58^{s}.18$, $\delta = 31°05'44''.8$. An optical spectrum of SSV 13, obtained by Goodrich (1986), shows a weak continuum, rising steeply towards the red, upon which are superimposed Hα, [O I] and [S II] emission lines, reminiscent of low-excitation HH objects. However, this spectrum may well be that of associated nebulosity rather SSV 13 itself.

CO observations over a large area by Snell & Edwards (1981) and Edwards & Snell (1983) have mapped a bipolar flow, the blueshifted lobe of which lies along and surrounds the HH objects and

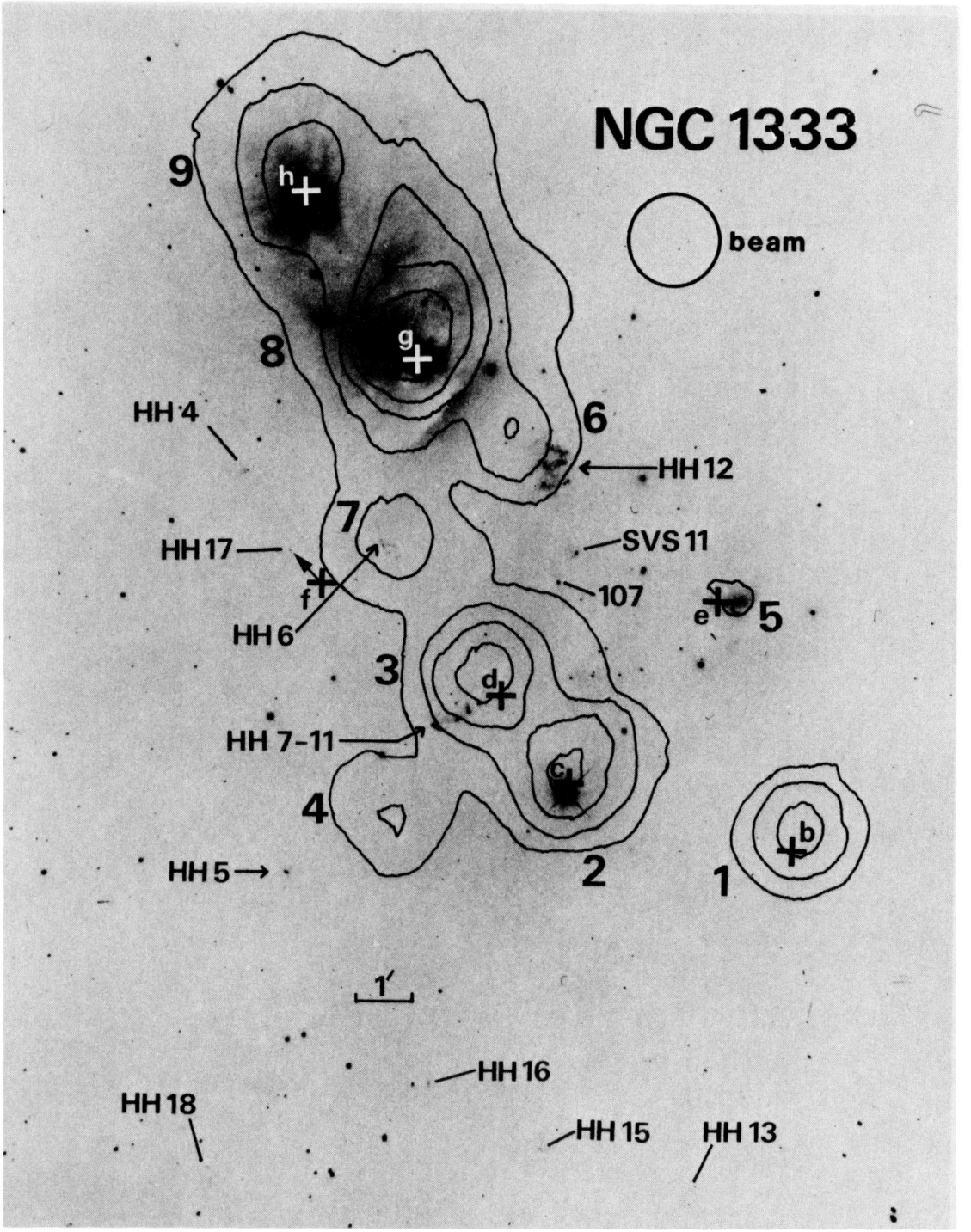

Plate 1. Optical map of the region (by kind permission of G. H. Herbig) with several 50 μm contours (levels 100, 170, 290, 490, 830 and 1400 MJy Ster^{-1}) superimposed. The point source detections are indicated by crosses and referred to by lower case letters, as listed in Table 2. The positions of several Herbig–Haro objects, together with stars SSV 11 and 107 (labelled SVS 11 and 107 respectively), have been indicated. The non-coincidence of the CPC flux peaks with the positions of the point sources is due to positioning uncertainties.

[*facing page* 464]

Table 1. *IRAS* Chopped Photometric Channel sources detected in the NGC 1333 region.

SOURCE	POSITIONS (1950) α	δ	FLUX DENSITY (Jy) 50μm	100μm	Temp K	Flux 10^{-12} Wm^{-2}	Luminosity $L_\odot$	Other Associations
IRAS 1	3 25 32.8	31 03 32	49	67	48±4	4	14	FIRSSE 42
IRAS 2	3 25 52.6	31 04 30	104	300	38±2	12	42	BD+30 547
IRAS 3	3 25 59.3	31 06 10	124	304	40±2	13	46	HH 7-11, SVS 13
IRAS 4	3 26 6.9	31 03 32	30	143	33±2	6	21	H_2O (C) & (D)
IRAS 5	3 25 40.3	31 07 49	2	<26	>26	1	3	SVS 9
IRAS 6	3 25 57.2	31 10 12	62	204	37±2	8	28	HH 12, SVS 12
IRAS 7	3 26 6.9	31 08 28	55	107	42±3	5	18	HH 6
IRAS 8	3 26 6.8	31 11 50	426	1089	39±2	46	161	SVS 3
IRAS 9	3 26 16.1	31 14 50	90	309	36±2	12	42	BD+30 549

Column 1 Source identification.
2 & 3 Equatorial coordinate of the peak 50μm flux of the source, accurate to about 30".
4 & 5 Total flux in each band, with a relative uncertainty of about 15%
6 Dust temperature, obtained assuming an emissivity α 1/λ.
7 Total infrared flux, accurate to about 30%.
8 Total infrared source luminosity, assuming a distance of 350 pc.
9 Objects with which the infrared source can be identified.

Table 2. Extract for the *IRAS Point Source Catalog* for the region defined in Fig. 1.

	α (1950) δ	ASSOCIATION	F_1 U_1	F_2 U_2	F_3 U_3	F_4 U_4	T_1/T_2	T_2/T_3	T_3/T_4
a	3 25 39.2 30 55 20		0.4 ( )	0.3 ( )	1.4 (9)	12.4 ( )			
b	3 25 32.7 31 3 12	IRAS 1	0.5 (7)	16.5 (6)	116.8 ( )	529.1 ( )	99		
c	3 25 51.3 31 4 25	IRAS 2	0.2 ( )	10.0 ( )	201.3 (13)	451.4 (14)		52	33
d	3 25 57.9 31 5 50	IRAS 3	13.2 (5)	50.3 (5)	247.3 (12)	946.7 ( )	146	65	
e	3 25 39.2 31 7 21	IRAS 5	1.3 (7)	3.0 (7)	0.4 ( )	437.9 ( )	159		
f	3 26 14.7 31 8 16	HH 17	0.6 (38)*	1.0 (35)	0.4 ( )	946.7 ( )	171		
g	3 26 4.7 31 11 41	IRAS 8	44.1 (5)	116.0 (5)	587.1 (5)	966.0 (13)	159	65	38
h	3 26 14.6 31 14 29	IRAS 9	7.7 (4)	5.8 (15)	108.5 (18)	946.7 ( )	232	52	

Column 1 is the point source identification used in Plate 1.

Columns F_1, F_2, F_3, F_4 give the flux in Janskys at 12, 25, 60 and 100 microns respectively. Underscored fluxes have an IRAS flux density quality flag of 3 (2 if marked *), corresponding to a reliable detection and only these fluxes have been colour corrected.

Columns U_1, U_2 etc. give the value of the percentage relative flux density uncertainty for the corresponding detection.

Columns labelled T_1/T_2 etc give values for the dust temperature obtained from the division of IRAS Survey Array bands 1 and 2 etc., assuming an emissivity $\propto 1/\lambda$. Temperatures are only quoted where fluxes in both bands have good data quality flags and are approximate to the extent that the colour correction was based on a black body spectrum.

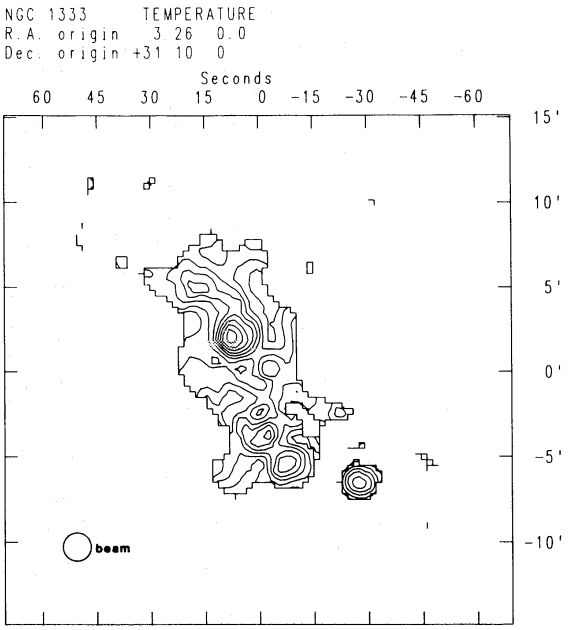

Figure 3. Dust temperature map obtained from the 50 and 100 μm data, assuming a dust emissivity $\propto 1/\lambda$. A minimum requirement of 80 MJy Ster^{-1} flux in each band was applied and this is indicated by the solid line enclosing the temperature contours. Contour levels are 35, 37, 39, 41, 43, 45, 47 and 49 K. Peak temperature contour for *IRAS* 1 and 8 is 49 K, and that for *IRAS* 3 is 45 K.

their powering source (no Herbig–Haro objects are observed in the redshifted lobe, prob because of the greater extinction into the cloud). SSV 13 is also associated with a water m H_2O(A) (Haschick *et al.* 1980). We measure the total IR luminosity in this region as 46 $L_\odot$ which compares well with the figure of 44 $L_\odot$ obtained by Harvey *et al.* when adjusted to a distance of 350 pc.

5.2 HH 12

HH 12, to the north-north-west of SSV 13 (*IRAS* 3), is a collection of Herbig–Haro objects of similar brightness to those in HH 7–11 (Plate 1). The closest IR source, SSV 12 (see Cohen &

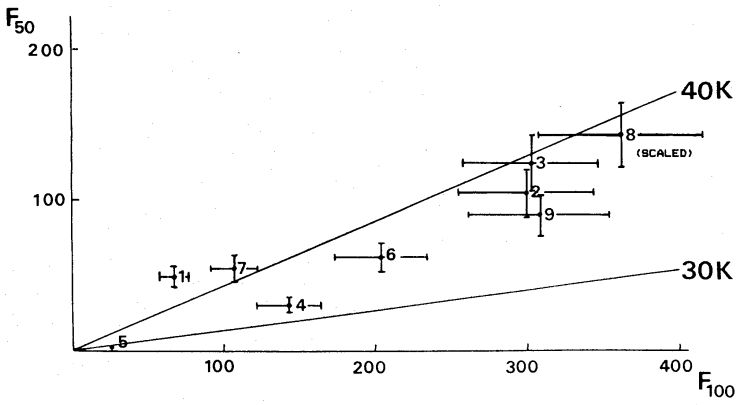

Figure 4. The flux in Janskys at 50 and 100 μm (F_{50} and F_{100}, respectively) of the sources listed in Table 1 have been plotted together with isothermal lines for 30 and 40 K (for an emissivity $\propto 1/\lambda$). *IRAS* 8 has been scaled down by a factor of 3 to include it in the plot. Error bars shown correspond to a (relative) uncertainty of 15 per cent in the fluxes.

Schwartz 1980) – here, *IRAS* 6 – lies to the east of the HH objects which have been shown to have velocities predominantly to the NNE (Herbig & Jones 1983). Although this source has an infrared luminosity of 28 $L_\odot$ and a dust temperature of 37 K, making it an ideal candidate for the energizing source, it is difficult to see how it can be responsible for the HH objects because their velocities are directed more towards *IRAS* 6 than away.

Several other possible candidates have been proposed as the driving force for HH 12. Herbig & Jones (1983), from the backward projection of the proper motions of some of the separate HH objects in the HH 12 association, suggested the star SSV 11 as the exciting source, whereas Strom, Strom & Stocke (1983) prefer the star SSS 107 on the basis of a tenuous line of Hα emission to HH 12. Neither of these stars are detected by the CPC observations which implies that there may be other candidates which are below the CPC detection level. A source which was detected in the vicinity was *IRAS* 5, a relatively weak source (~3 $L_\odot$) about 3.5 arcmin from HH 12 and which is associated with some reflection nebulosity. There is also the possibility that SSV 13 is playing a role in the energetics of HH 12, being only a little further away (4 arcmin) and having a much greater luminosity (46 $L_\odot$); while the CO outflows do not support this idea it is interesting to note that the direction of movement of component *F* of HH 12 (Herbig & Jones 1983) back projects to this star.

5.3 HH 6

HH 6 is coincident with our low-luminosity source *IRAS* 7. No exciting source has previously been identified with HH 6, which is associated with a water maser (Henkel, Haschick & Güsten 1986) and also with a radio continuum source which has recently been detected by Snell & Bally (1986). Snell & Bally propose that, in cases of low-luminosity sources, the radio emission can result from high-velocity outflow in a stellar wind. The luminosity of *IRAS* 7, 18 $L_\odot$, and the presence of HH 6 confirms that this is a likely scenario in this case.

5.4 HH 17

No significant far-IR emission was detected in the immediate vicinity of HH 17 by the CPC, however its position is coincident with the 12 and 25 μm point source detections (*f*, Plate 1) by the *IRAS* survey array (Table 2). These fluxes are consistent with the possibility that the source was too weak to be detected at 60 μm. However, as the adjacent source *IRAS* 7 (90 arcsec from HH 17) is not present in the *IRAS Point Source Catalog*, there exists the possibility that the point source detection at the position of HH 17 is being confused with nearby *IRAS* 7. In an attempt to determine exactly why *IRAS* 7 and 6 (mentioned above in connection with HH 12) are not in the point source catalogue, *IRAS* sky flux and survey raw data of the region were inspected. We conclude that neither of these sources were detected in the survey processing due to their proximity to the bright source *IRAS* 8 and the lower resolution of the survey arrays.

It is interesting to note that the north–south ridge of 100 μm emission in this region (Fig. 2) could be associated with the exciting stars for HH 17 and 4.

5.5 HH 5, 13, 15, 16, 18

No significant far-IR emission was detected in the vicinity of any of the other single HH objects scattered around NGC 1333. For a typical dust colour temperature of 35 K, this gives a 10σ upper limit for the powering stars of about 3 $L_\odot$.

5.6 POSSIBLE PROTOSTELLAR CANDIDATES

In this region of known star formation, we have searched for evidence of protostellar candidates. In such a search the first objective must be the formulation of a definition of what constitutes a protostellar object. In their review, Bodenheimer & Black (1978) have defined such objects as those having surface temperatures less than 3000 K and which are following a Hayashi track in the HR diagram. Infrared observations will be important to the identification of these objects since during collapse (and accretion) the protostar will be obscured optically by infalling cold dust and gas. The relationship between circumstellar material, which may be accreting on to the central core, and outflows has not been well established. Some models (e.g. Torbett 1984) involve a protostellar accretion disc generating its own outflow as a natural product. Pudritz & Norman (1986) have also proposed such a model which they have used to obtain masses, rotation rates and densities for several regions including HH 7–11. Such models are required to explain the extraction of angular momentum from the central rotating body. On the other hand, it has been suggested by Lada (1985) that an object in which inflow is still continuing is unlikely to be involved in mass outflow with its associated phenomena, such as Herbig–Haro objects. In this case the onset of this phase marks the end of star formation and the beginning of stellar evolution, and, as such, suitable protostellar candidates should be identified as dense cores of material not associated with significant outflows, or Herbig–Haro objects and observed by virtue of the thermal emission from the surrounding relatively low-temperature dust.

An aid to resolving the issue of the onset of molecular outflow might come from further study of *IRAS* 1, a promising protostellar candidate. It has a bolometric luminosity of $14\,L_{\odot}$ and a relatively high apparent dust temperature of 48 K. It is highly obscured with no apparent association with any Herbig–Haro objects and yet CO observations of the $v=3$–2 and $v=2$–1 lines show that it has significant outflow of gas, as recently observed by White (1986, private communication).

Applying the model of Pudritz & Norman (1986), this would suggest that *IRAS* 1 is a very young object indeed, since we may well be observing it at a stage after the molecular outflow has begun but before the onset of an optical jet. *IRAS* 1 is probably the source designated FIRSSE 42 (Price, Murdock & Shivanandan 1983), although the respective positions differ by more than 2.5 arcmin in declination. FIRSSE 42 has a flux of 272 Jy at 93 μm compared with the *IRAS* CPC 100 μm flux of 67 Jy, but this discrepancy can be attributed to the large difference in beam sizes – the FIRSSE search involved a 5.3×12 arcmin^2 beam.

Another possible protostellar candidate is *IRAS* 4 which, although radiating significant flux in both wavebands, does not have a pronounced peak on the temperature map. As this source is not significantly warmer than its surroundings, it could be a condensation which radiates more flux because of its greater optical depth or it could possibly be a protostellar object.

The coincidence of two water maser sources H_2O (C) (Haschick *et al.* 1980) and H_2O (D) (Ho *et al.* 1982) in the vicinity of *IRAS* 4 adds weight to the latter possibility, since the presence of such masing sources in regions of ongoing star formation is thought to be indicative of mass outflows in the extended envelopes of young stars and Sandell & Liseau (1986, private communication) have recently discovered CO outflows near *IRAS* 4, confirming further the protostellar hypothesis. The masers in *IRAS* 4 require a source of strong IR radiation, which would be supplied by the dusty young star, to act as a pumping mechanism to maintain population inversion in the high-density H_2O region in the vicinity of the star. The separation of the two masers associated with *IRAS* 4 is 1 arcmin, implying that they may be independently pumped by different sources. As such, *IRAS* 4 may well be two heavily embedded sources, lying close enough together in the plane of the sky, to have not been resolved by the CPC. The region is certainly highly active, contrary to what is observed optically, and is of considerable interest.

5.7 MAIN OR NEARLY MAIN-SEQUENCE STARS

The most luminous IR source in the region is *IRAS* 8 at the location of the star SSV 3 which is powering the IR output. Harvey *et al.* (1984) note that the overall energy distribution of this star, based on 1–160 μm data, resembles that of Herbig Ae–Be objects. They obtain a value of 176 $L_\odot$ at 350 pc, again in line with our CPC value of 161 $L_\odot$.

IRAS 9 corresponds to the star BD+30°549, which Harvey *et al.* (1984) have shown to be the least reddened of the four IR sources that they observed in NGC 1333. In this case the overall data are consistent with the star being a nearly main-sequence late B star embedded in a diffuse cloud, similar to other reflection nebulae which are sources of weak, diffuse far-IR emission. Harvey *et al.* (1984) show that the measured IR radiation represents only a small fraction of the luminosity of the star.

IRAS 5 is a relatively weak source with $L \sim 3\ L_\odot$ which has already been mentioned in the above section on HH 12. It appears to be associated with SSV 9 and the nebulosity which can be seen on the photograph (Plate 1).

IRAS 2 is coincident with the visible star BD+30°547, although this is likely to be a foreground star.

6 Conclusions

(i) The maps at 50 and 100 μm obtained with the Chopped Photometric Channel on *IRAS* show more structure than has previously been observed for the NGC 1333 region. The area of the maps was completely covered as a tight raster scan was used for the observations. Nine far-IR sources have been separated from the background, some of which – *IRAS* 1, 4, 5 and 7 – have not been reported prior to these observations. Of the sources for which it is possible to compare luminosities, those reported here agree well with previous observations.

(ii) The relationship between evolving stars and Herbig–Haro objects can clearly be seen for some of the sources (e.g. *IRAS* 3 and 7), but the star responsible for the HH 12 association has not been unambiguously identified.

(iii) The region scanned by the CPC contains many HH objects for which no exciting star has been detected (e.g. HH 5, 13, 15, 16 and 18). This implies that the luminosity of these sources must be well below the 10σ detection limit of about 3 $L_\odot$. The star (*f*, Plate 1) which could be associated with HH 17, although not detected by the CPC, was sufficiently bright at 12 and 25 μm to be observed by the *IRAS* survey array.

(iv) *IRAS* 1, with its molecular outflow, is thought to be a good protostellar candidate. *IRAS* 4 being cooler than the other sources detected, may contain a protostar or protostars at an even earlier stage.

(v) The overall results of this investigation are summarized in Fig. 4 which is a flux–flux plot. Lines corresponding to radiation from dust at 30 and 40 K are shown, assuming an emissivity proportional to $1/\lambda$. These fluxes are from the outer layers of dust which have been heated by partial or total absorption of the radiation from the central source. It can be seen that the dust temperatures cluster principally around the 40 K line, the hottest ones corresponding to sources such as 1, 3, and 7 which have known outflows. Other sources with outflows, e.g. *IRAS* 4, are somewhat cooler, possibly due to being at an earlier stage in their development.

Acknowledgments

It is a pleasure to thank all who helped to make the *IRAS* mission so successful, in particular the members from the Netherlands who provided the CPC and prepared the final data from that

instrument. We very much appreciate receiving the results of the CO observations on source No. 1 from Dr Glenn White prior to publication.

The authors are also grateful for useful discussions with Drs K. J. King and J. F. Lightfoot and also with the *IRAS* Post Mission Analysis Facility Team at the Rutherford Appleton Laboratory.

We also thank Drs R. Liseau and G. Sandell for supplying us with details of their recent CO survey of this region and for their useful comments.

DHMC acknowledges the studentship provided by the Department of Education for Northern Ireland.

References

Beichman, C. A. Neugebauer, G., Habing, H. J., Clegg, P. E. & Chester, T. J. (eds), 1985. *Explanatory Supplement to the IRAS Catalogs and Atlases,* GPO, Washington.

Bodenheimer, P. & Black, D. C., 1978. *Protostars and Planets I,* p. 288, ed. Gehrels, T., University of Arizona Press.

Cohen, M. & Schwartz, R. D., 1980. *Mon. Not. R. astr. Soc.*, **191,** 165.

Edwards, S. & Snell, R. L., 1983. *Astrophys. J.,* **270,** 605.

Goodrich, R. W., 1986. *Astr. J.,* **92,** 885.

Harvey, P. M., Wilking, B. A. & Joy, M., 1984. *Astrophys. J.,* **278,** 156.

Haschick, A. D., Moran, J. M., Rodriguez, L. F., Greenfield, P. & Garcia-Barreto, J. A., 1980. *Astrophys. J.,* **237,** 26.

Ho, P. T. P., Haschick, A. D., Moran, J. M. & Rodriguez, L. F., 1982. *Bull. Am. astr. Soc.,* **14,** 927.

Henkel, C., Haschick, A. D. & Güsten, R., 1986. *Astr. Astrophys.,* **165,** 197.

Herbig, G. H. & Jones, B. F., 1983. *Astr. J.,* **88,** 1040.

Lada, C. J., 1985. *Ann. Rev. Astr. Astrophys.,* **23,** 267.

Lightfoot, J. F. & Glencross, W. M., 1986. *Mon. Not. R. astr. Soc.,* **221,** 993.

Liseau, R., 1985. *PhD thesis,* University of Stockholm.

Mundt, R., 1985. In: *Protostars and Planets II,* p. 414, eds Black, D. & Matthews, M., University of Arizona Press.

Neugebauer, G. *et al.*, 1984. *Astrophys. J.,* **278,** L1.

Price, S. D., Murdock, T. L. & Shivanandan, K., 1983. *AFGL-TR-83-0055.*

Pudritz, R. E. & Norman, C. A., 1986. *Astrophys. J.,* **301,** 571.

Snell, R. L. & Bally, J., 1986. *Astrophys. J.,* **303,** 683.

Snell, R. L. & Edwards, S., 1981. *Astrophys. J.,* **251,** 103.

Strom, S. E., Grasdalen, G. L. & Strom, K. M., 1974. *Astrophys. J.,* **191,** 111.

Strom, K. M., Strom, S. E. & Stocke, J., 1983. *Astrophys. J.,* **271,** L23.

Strom, S. E., Vrba, F. J. & Strom, K. M., 1976. *Astr. J.,* **81,** 314.

Torbett, M., 1984. *Astrophys. J.,* **278,** 318.

Wesselius, P. R. *et al.*, 1985. *IRAS Chopped Photometric Channel Explanatory Supplement,* Laboratory for Space Research, Groningen, Holland.

Wildeman, K. J., Beintema, D. A. & Wesselius, P. R., 1983. *J. Brit. Interplanet. Soc.,* **36,** 21.

Zealey, W. J., Williams, P. M. & Sandell, G., 1984. *Astr. Astrophys.,* **140,** L31.